




Article

Diagnostic Performance and Radiation Dose of the EOS System to Image Enchondromatosis: A Phantom Study

Domenico Albano ^{1,2}, Alessandro Loria ³, Cristiana Fanciullo ⁴, Alberto Bruno ⁵, Carmelo Messina ^{1,6}, Antonella del Vecchio ³ and Luca Maria Sconfienza ^{1,6,*}

¹ IRCCS Istituto Ortopedico Galeazzi, 20161 Milano, Italy; albanodomenico@me.com (D.A.); carmelomessina.md@gmail.com (C.M.)

² Sezione di Scienze Radiologiche, Dipartimento di Biomedicina, Neuroscienze e Diagnostica Avanzata, Università di Palermo, 90127 Palermo, Italy

³ Servizio di Fisica Sanitaria, IRCCS Ospedale San Raffaele, 20132 Milano, Italy; loria.alessandro@hsr.it (A.L.); delvecchio.antonella@hsr.it (A.d.V.)

⁴ Postgraduate School of Diagnostic and Interventional Radiology, University of Milan, 20122 Milano, Italy; fanciullo.cristiana@gmail.com

⁵ Centro Salus, 90145 Palermo, Italy; bruno-alberto@hotmail.it

⁶ Dipartimento di Scienze Biomediche per la Salute, Università degli Studi di Milano, 20133 Milano, Italy

* Correspondence: io@lucasconfienza.it; Tel.: +39-02-66214004

Received: 29 October 2020; Accepted: 9 December 2020; Published: 15 December 2020



Abstract: Background: Radiation doses and capability of EOS, conventional radiography (CR), and computed tomography (CT) to detect and measure enchondromas in a dedicated five-year-old anthropomorphic phantom were compared. Methods: To simulate enchondromas, minced pieces of chicken bone and cartilage were packed in conventional kitchen plastic foil to create ovoidal/rounded masses and randomly hung on the phantom. The phantom was imaged five times with CR, CT, and EOS, each time changing the number and position of inserts. All images were reviewed by a senior radiologist and a radiology resident. Results: EOS and CR detected all inserts in 4/5 cases (80%), while in one case 1/17 inserts was not seen. Excellent agreement of EOS with CR (88% reproducibility; bias = 14 mm; repeatability coefficient (CoR) 2.9; 95% CI from −2.8 to 3.1 mm; $p = 0.5$) and CT (81% reproducibility; bias = 15 mm; CoR 5.2; 95% CI from −5.5 to 5.2 mm; $p = 0.7$) was found. EOS showed 71% interobserver reproducibility (CoR 7.2; bias = 0.6 mm; 95% CI from −6.6 to 7.8 mm; $p = 0.25$). The EOS-Fast radiation dose was also significantly lower than the median radiation dose of CR (644.7 (599.4–651.97) mGy•cm², $p = 0.004$). Conclusions: Low-dose EOS has the same capability as CR to detect and measure enchondroma-like inserts on a phantom and may be considered to monitor patients with multiple enchondromas.

Keywords: EOS; conventional radiography; computed tomography; radiation dose; enchondroma; phantom

1. Introduction

Enchondromas are common, benign cartilage tumors that mostly develop in the metaphysis of long bones in close proximity to growth plate cartilage [1–5]. Ollier disease, also known as enchondromatosis, is a nonhereditary disorder defined by the presence of multiple enchondromas, while Maffucci syndrome is that condition in which multiple enchondromatosis is associated with soft tissue hemangiomas [6]. The prevalence of Ollier disease is estimated to be 1/100,000, while there are about 200 reports of Maffucci syndrome. Both conditions usually present during childhood as a possible consequence of a differentiation disorder during endochondral ossification of growth plate tissue [7]. Clinical problems caused by enchondromas depend on the extent of skeletal involvement

and include skeletal deformities associated or not with pathological fracture, limb-length discrepancy, and the potential risk for malignant transformation to chondrosarcoma [3–5]. The diagnosis of Ollier disease is mainly based on clinical and radiological evaluations, which typically show an irregular distribution of multiple, radiolucent, homogenous lesions with an oval or elongated shape and a well-defined, slightly thickened bony margin. Since children affected by Ollier disease will undergo multiple radiographs during childhood for diagnosis and follow-up, the need for accurate assessment of enchondromas has to balance with the risks associated with repeated radiation exposure. Repeated exposure of children to radiation is a major concern, having been reported to be 2 to 5 times more radiosensitive than adults [8] and to have the highest risk of cancer development, as radiologic stochastic damage has a latency of one or even two decades. Thus, in the last few decades, much effort has gone into developing radiologic techniques able to keep radiation doses “as low as reasonably achievable” (ALARA), while not compromising image quality, especially in pediatric imaging [9].

EOS (EOS Imaging, Paris, France) is a relatively novel low-dose imaging system that is capable of producing radiographic images with very low radiation exposure [10]. It exploits a biplanar slot-scanning technology that employs highly sensitive gaseous photon detectors [11–13]. It consists of a cabin in which the patient is positioned standing erect, and the two linear X-ray sources and two gaseous detector arrays allow for the patient to be scanned in two orthogonal planes simultaneously. The X-ray sources move in synchronous fashion so that the beam is always horizontal to the patient, thus avoiding the magnification error (the so-called “parallax effect”) of teleradiography. Once acquisition parameters have been set on the basis of three predefined morphotypes, the scan can start. The scan has a variable duration of up to twenty seconds, making this modality sensitive to motion artifacts. However, the acquisition can be shortened, further minimizing the dose with minimal reduction of image quality [14].

In general, the EOS system is excellent in the evaluation of biomechanical alignment of the spine and of the lower limbs, while it is not routinely used in the evaluation of focal bone lesions. Indeed, the diagnostic accuracy of the EOS system to identify and measure bone tumors has not been investigated previously. Moreover, the reduction of dose obtained by the EOS system has been established. Nevertheless, this exam can be acquired with different speeds, which are associated with different radiation doses and image quality, but a comparison of radiation doses of different sets of EOS images and conventional radiography to image the whole skeletal system has not been previously reported. The rationale for conducting this study was the lack of data concerning the potential use of this low-dose imaging examination to follow patients with multifocal bone lesions, namely enchondromatosis, in order to decrease the radiation burden on young patients affected by these conditions but providing images with enough quality to be used for oncologic purposes. Thus, the objective of this study was to compare radiation doses and the capability of the EOS imaging system with those of conventional radiography and computed tomography (CT) to detect and measure enchondromas in a dedicated phantom.

2. Materials and Methods

2.1. Study Design

Institutional review board approval was not needed since no humans were involved in the present study. This report is concerned with the comparison of radiation doses and the capability of the EOS imaging system, a conventional radiographic system, and a CT system to detect and measure enchondromas in a dedicated five-year-old anthropomorphic phantom (ATOM Dosimetry Verification Phantom, Model 705; pediatric 5 years; height = 110 cm; weight = 19 kg; physical density = 1.52 g/cm³; electron density = 4.801 × 10²³). This phantom is routinely used to perform radiation dose measurements. To simulate enchondromas, minced pieces of chicken bone and cartilage were packed in conventional kitchen plastic foil to create ovoidal/rounded masses. The inserts had a shortest diameter ranging from 1.3 cm to 3.8 cm and a longest diameter ranging from 2 cm to

4.9 cm. They were randomly hung on the phantom anteriorly, posteriorly, and laterally to simulate a real irregular disposition of multiple enchondromas. The phantom was imaged with the use of conventional radiography, CT, and EOS radiographic imaging. Anteroposterior (AP) and laterolateral (LL) conventional radiography and EOS images, as well as CT scans, were performed five times. Each time the number and position of inserts were changed, hanging 3, 6, 9, 16, and 17 inserts on the phantom, respectively. The phantom was configured by a physicist who was then not involved in image analysis.

2.2. Conventional Radiography

Full-length long radiographs of the phantom were made with direct digital acquisition using a Siemens Ysio Max X-ray machine (Siemens AG, Erlangen, Germany) and a Fuji imaging machine (FujiFilm, Stamford, CT) (35.4 × 124.5 cm) behind a standard bucky grid. The phantom was secured to an Octostop immobilizer (Octostop, QC, Canada) with Velcro straps in a vertical orientation and was positioned directly in front of the grid and cassette with the front of the phantom directed anteriorly toward the X-ray source. The X-ray parameters were set automatically by the system.

2.3. Computed Tomography

The phantom was positioned in the center of a 64-slice Siemens CT scanner (Definition AS+, Siemens Healthcare, Forchheim, Germany). The phantom was subjected to a whole-body CT scan from head to feet with the following acquisition parameters: 120 kV; 60 mA; slice thickness 1 mm; pitch 0.8.

2.4. EOS

Different sets of radiographs were made with the EOS scanner. The phantom was fixed with Velcro straps to an Octostop immobilizer and was placed with a vertical orientation in the scanning chamber. The phantom was aligned with laser-light markings to ensure that the anterior side was oriented anteriorly and in the center of the scanning field.

For radiation dose evaluation, three sets of imaging parameters (with 200 mA, 83 kV for AP images and 102 kV for LL images) were used: (1) a slow setting (speed setting 4, 7.6 cm/s), (2) a medium setting (speed setting 3, 11.4 cm/s), and (3) a fast ultralow-dose setting (speed setting 2, 15.2 cm/s). For each configuration of the inserts (i.e., 3, 6, 9, 16, and 17 inserts) and for each set of image parameters, one AP and one LL view were acquired. Thus, a total of 15 AP and 15 LL images of the phantom were acquired, with the phantom being removed and repositioned after each image was made. Only EOS-Fast images were reviewed to detect and to measure the enchondromas-like inserts, while EOS-Medium and EOS-Slow images were used to compare the radiation doses of the different sets of images.

2.5. Image Analysis

All images were downloaded to a picture-archiving and communication system (Andra, Stockholm, Sweden). A radiologist with more than five years of experience in musculoskeletal radiology and research and a radiology resident reviewed the images in a random order and blinded to the number of inserts and type of scan (for EOS images). The number of inserts visible on each image was counted and their size was measured using an electronic caliper.

2.6. Statistical Analysis

The continuous variables are reported as means ± standard deviations. Intermodality and interobserver reproducibility were tested by using the Bland–Altman method [15]. The radiation doses in terms of Kerma-area product (KAP) [16], calculated from both conventional radiography and EOS system examinations, are reported as medians ± interquartile ranges, and differences were analyzed using the Mann–Whitney *U* test. A *p*-value less than 0.05 was considered statistically significant,

where appropriate [17]. Statistical analysis was performed using SPSS software (v. 25, IBM, Armonk, NY, USA).

3. Results

3.1. Diagnostic Accuracy

Seventeen different inserts were used for this experiment, whose dimensions ranged from 20 × 14 mm to 49 × 34 mm.

The two different readers measured the longest insert length, with both EOS and conventional radiography obtaining values ranging from 7 mm to 40 mm with the EOS system and from 6 mm to 36 mm with conventional radiography. Both conventional radiography and EOS underestimated the true length of the inserts by an average of 6.6 mm (25.2%) and 6.1 mm (23.9%), respectively, when compared with the true length of a respective insert on its longest axis. The comparison of the mean difference between the measurements for both modalities and the true length is reported in Table 1.

Table 1. Insert length measurements with EOS and CR.

	EOS Imaging System	Conventional Radiography
Difference from true length of phantom inserts (mm) *	−6.1 (from −18 to +1)	−6.6 (from −19 to +1.5)
Relative magnification **	−23.9%	−25.2%

* The values indicate the difference from the true length of the phantom inserts as provided by the manufacturer and are expressed as the mean, with the range in parentheses. ** The relative magnification was derived by dividing the difference between the measured length and the true length by the true length.

Both observers were able to detect the same number of inserts per phantom on EOS and conventional radiography: This was equal to the number of inserts placed on the phantom in 4/5 cases (80%), while in one case, 1 out of 17 inserts was not seen. On CT, both observers always detected the correct number of inserts, as compared to the real number (Table 2).

Table 2. Number of inserts detected per phantom on the three imaging modalities by two different observers who reviewed all images independently.

Phantom	Observer 1			Observer 2		
	n. Inserts CT	n. Inserts EOS	n. Inserts CR	n. Inserts CT	n. Inserts EOS	n. Inserts CR
# 1	16	16	16	16	16	16
# 2	17	16	16	17	16	16
# 3	3	3	3	3	3	3
# 4	6	6	6	6	6	6
# 5	9	9	9	9	9	9
Total	51	50	50	51	50	50

Intermodality reliability, quantified as the mean of the difference between the two modalities' measurements (bias) and the repeatability coefficient (CoR), showed excellent agreement for EOS, conventional radiography, and CT with a bias calculated to be 0.14 mm (88% reproducibility; CoR 2.9; 95% CI from −2.8 to 3.1 mm; $p = 0.5$) and 0.15 mm (81% reproducibility; CoR 5.2; 95% CI from −5.5 to 5.2 mm; $p = 0.7$) when comparing EOS to conventional radiography and CT, respectively. The assessment of interobserver reliability in the EOS modality showed 71% reproducibility between different observers, with a bias as low as 0.6 mm (CoR 7.2; 95% CI from −6.6 to 7.8 mm; $p = 0.25$) (Figure 1).

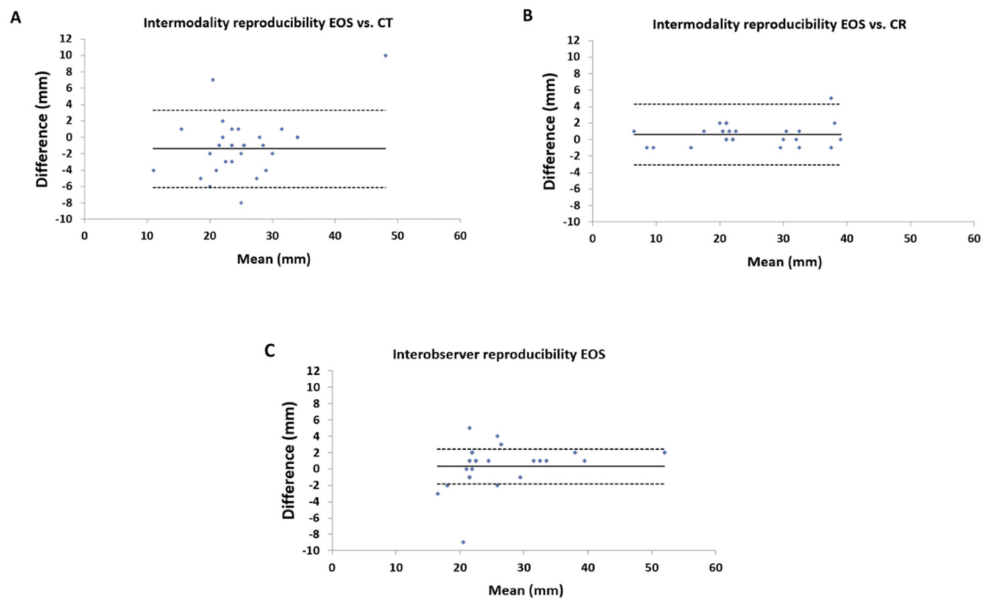


Figure 1. Intermodality and interobserver reliability of insert length measurements among different modalities and among different observers: (A) Intermodality reliability between EOS imaging system and computed tomography (CT) scanning. The mean of the measurements obtained with EOS and CT for each insert is reported on the x-axis; the difference between the two measurements is reported on the y-axis. (B) Intermodality reliability between the EOS imaging system and conventional X-ray. The mean of the measurements obtained with EOS and X-ray for each insert is reported on the x-axis; the difference between the two measurements is reported on y-axis. (C) Interobserver reliability between measurements obtained by two different observers with the EOS imaging system. The mean of the measurements is reported on the x-axis; the difference between them is reported on the y-axis.

3.2. Radiation Dose

By applying different image scanning speeds, the radiation dose delivered was progressively and significantly lower for the EOS-Fast protocol (KAP 258.6 mGy cm²) compared with the EOS-Medium protocol (KAP 387.89 mGy cm², $p < 0.001$), and even more when compared with the EOS-Slow protocol (KAP 517.19 mGy cm², $p < 0.001$) (Figure 2). Moreover, the EOS-Fast radiation dose was also significantly lower than the median radiation dose of conventional radiographs (644.7 (599.4–651.97) mGy cm², $p = 0.004$) for all phantom configurations (Figure 3). Figure 4 shows a case from this study.

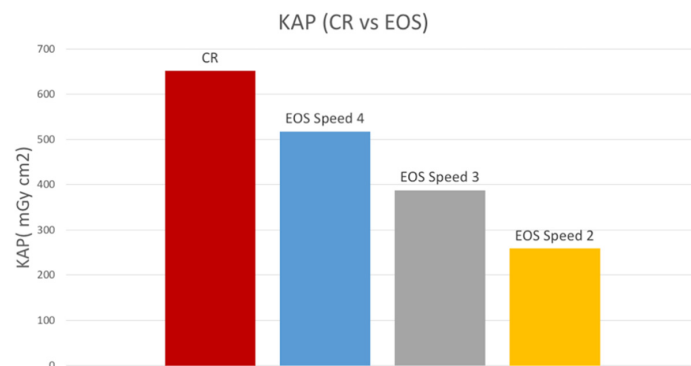


Figure 2. Bar graph illustrating the mean radiation dose by modality. CR = conventional radiographs and EOS = EOS imaging system at three different speed settings (speed 2 = 15.2 cm/s; speed 3 = 11.4 cm/s; speed 4 = 7.6 cm/s).

Configuration	EOS Speed	KAP (mGy cm ²)	
		EOS	CR
1	4	517.19	402.2
	3	387.89	
	2	258.6	
2	4	517.19	261.8
	3	387.89	
	2	258.6	
3	4	517.19	599.4
	3	387.89	
	2	258.6	
4	4	517.19	654.4
	3	387.89	
	2	258.6	
5	4	517.19	644.7
	3	387.89	
	2	258.6	

Figure 3. Radiation doses delivered by the EOS-Fast (speed 2), EOS-Medium (speed 3), and EOS-Slow (speed 4) protocols, and CR examinations.

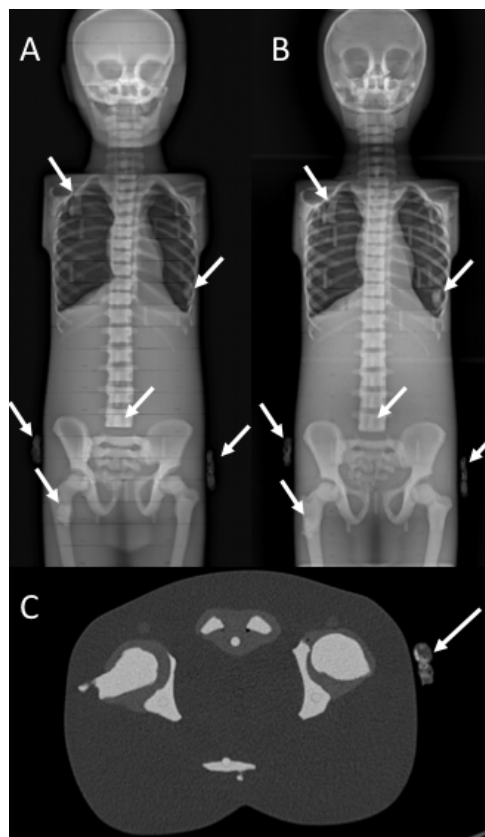


Figure 4. EOS (A), CR (B), and CT (C) images of a phantom with six inserts (arrows).

4. Discussion

The results from this study indicate that EOS performs similarly to conventional radiography in both number detection and length evaluation of enchondroma-like inserts in a standardized phantom setting. The mean difference between insert length assessed with EOS and conventional radiography, and their true length was in fact as low as 6.1 mm and 6.6 mm, respectively. However, it should be underlined that an underestimation of the insert size was expected, in view of the bidimensional imaging provided by both techniques that does not make a precise identification of the longest diameter

of the inserts possible. Notably, these results were obtained by testing the capability of the reviewers to detect and measure the enchondroma-like inserts on EOS fast-speed images, which should present minimal reduction of image quality when compared with the other sets of EOS images.

The intermodality reliabilities of EOS imaging, conventional radiography, and CT were also excellent, which is essential when dealing with a new diagnostic test not yet used in the clinical routine [18]. Moreover, perfect agreement of measurements performed by different observers with the EOS system was observed, thus demonstrating that EOS is both accurate and reproducible. There was only a single case where the number of inserts was different between conventional radiography and EOS versus CT and the actual number of inserts placed on the phantom. In this case, two inserts were placed very close to one another. Thus, the bidimensional images of conventional radiography and EOS showed them almost superimposed on one another, making the distinction almost impossible.

This study also demonstrates that, since radiation dose is inversely related to scanning speed, you can impact the radiation dose administered by the EOS system by changing the speed of the image-acquisition parameters. Indeed, doubling the speed from EOS-Slow (7.6 cm/s) to EOS-Fast (15.2 cm/s), the radiation dose decreased from 517.19 mGy cm² to 258.6 mGy cm² without affecting the capability of observers to detect and measure the inserts on the phantom. These data lead us to consider EOS as a potential imaging tool technique for detecting and following enchondromas over time, while minimizing radiation exposure. A drawback of EOS to consider is the increased risk of motion artifacts related to the fact that EOS is performed with the patient in a standing position and the acquisition time at a speed setting of 4 is about 8 s. This should be considered especially in pediatric patients who are particularly prone to movement during a scan. This limitation can be partly overcome, given that image-acquisition time can be decreased to three to four seconds (on the EOS-Fast speed setting of 2) without affecting the capability of observers to detect and measure the inserts on a phantom.

In the future, we may envision a clinical setting where initial evaluation of enchondromas is performed using conventional radiography and follow-up is performed using EOS. In case of a change in the number and size of enchondromas, a standard workup should then be resumed. Clearly, one limitation of this approach is that EOS is not a widely available imaging modality.

A limitation of this work is that the image quality of conventional radiography was not compared with that of EOS at different acquisition speeds. It is known that EOS is very good in assessing spine and limb orientation, but, especially at higher speeds, image quality may also decrease in favor of radiation dose reduction. However, the excellent results of this study were obtained by testing the capability of the reviewers to detect and measure the enchondroma-like inserts on EOS fast-speed images, which should have had reduced image quality when compared with the other sets of EOS images. Also, the enchondroma-like inserts were attached on the external surface (i.e., the “skin”) of the phantom, which is not exactly what happens in enchondromatosis. However, this was the best approximation possible, as the anthropomorphic phantom is not empty and lesions cannot be placed inside its body.

In conclusion, low-dose EOS digital radiographic evaluation has the same capability as conventional radiography to detect and measure enchondroma-like inserts on a phantom. Thanks to its lower radiation dose, this method may be considered in the follow-up of patients with multiple enchondromas. However, clinical studies are warranted to confirm these preliminary results on a phantom.

Author Contributions: Conceptualization, D.A., A.d.V., and L.M.S.; methodology, D.A., C.M., A.L., A.d.V., and L.M.S.; formal analysis, D.A., C.F., A.B., C.M., and L.M.S.; investigation, D.A. and A.B.; data curation, D.A., A.L., A.B., C.F., and L.M.S.; writing—original draft preparation, D.A. and C.F.; writing—review and editing, C.M., A.L., A.d.V., and L.M.S.; supervision, L.M.S. All authors have read and agreed to the published version of the manuscript.

Funding: This research received no external funding.

Conflicts of Interest: The authors declare no conflict of interest.

References

1. Albano, D.; Messina, C.; Gitto, S.; Papakonstantinou, O.; Sconfienza, L.M. Differential Diagnosis of Spine Tumors: My Favorite Mistake. *Semin. Musculoskelet. Radiol.* **2019**, *23*, 26–35. [[CrossRef](#)] [[PubMed](#)]
2. Gitto, S.; Cuocolo, R.; Albano, D.; Chianca, V.; Messina, C.; Gambino, A.; Ugga, L.; Cortese, M.C.; Lazzara, A.; Ricci, D.; et al. MRI radiomics-based machine-learning classification of bone chondrosarcoma. *Eur. J. Radiol.* **2020**, *128*, 109043. [[CrossRef](#)] [[PubMed](#)]
3. Maroteaux, P.; Le Merrer, M. *Les Maladies Osseuses de L'enfant*; Médecine-Sciences Flammarion: Paris, France, 2002.
4. Unni, K.K. Cartilaginous lesions of bone. *J. Orthop. Sci.* **2001**, *6*, 457–472. [[CrossRef](#)] [[PubMed](#)]
5. Whyte, M. Acquired disorders of cartilage and bone. *Am. Soc. Bone Miner. Res.* **2003**.
6. Fletcher, C.D.M.; Unni, K.K.; Mertens, F. *Pathology and Genetics of Tumours of Soft Tissue and Bone*; Iarc: Lyon, France, 2002; Volume 4.
7. Hopyan, S.; Gokgoz, N.; Poon, R.; Gensure, R.C.; Yu, C.; Cole, W.G.; Bell, R.S.; Jüppner, H.; Andrulis, I.L.; Wunder, J.S.; et al. A mutant PTH/PTHrP type I receptor in enchondromatosis. *Nat. Genet.* **2002**, *30*, 306–310. [[CrossRef](#)] [[PubMed](#)]
8. Strauss, K.J.; Kaste, S.C. ALARA in pediatric interventional and fluoroscopic imaging: Striving to keep radiation doses as low as possible during fluoroscopy of pediatric patients—A white paper executive summary. *J. Am. Coll. Radiol.* **2006**, *3*, 686–688. [[CrossRef](#)] [[PubMed](#)]
9. The 2007 Recommendations of the International Commission on Radiological Protection. ICRP publication 103. *Ann. ICRP* **2007**, *37*, 1–332.
10. Melhem, E.; Assi, A.; El Rachkidi, R.; Ghanem, I. EOS((R)) biplanar X-ray imaging: Concept, developments, benefits, and limitations. *J. Child. Orthop.* **2016**, *10*, 1–14. [[CrossRef](#)] [[PubMed](#)]
11. Dubouset, J.; Charpak, G.; Dorion, I.; Skalli, W.; Lavaste, F.; Deguise, J.; Kalifa, G.; Ferey, S. A new 2D and 3D imaging approach to musculoskeletal physiology and pathology with low-dose radiation and the standing position: The EOS system. *Bull. Acad. Natl. Med.* **2005**, *189*, 287–300. [[PubMed](#)]
12. Dubouset, J.; Charpak, G.; Skalli, W.; Kalifa, G.; Lazennec, J.-Y. EOS stereo-radiography system: Whole-body simultaneous anteroposterior and lateral radiographs with very low radiation dose. *Revue de Chirurgie Orthopedique et Reparatrice de L'appareil Moteur* **2007**, *93*, 141–143. [[CrossRef](#)]
13. Albano, D.; Messina, C.; Gambino, A.; Gurgitano, M.; Sciabica, C.; Oliveira Pavan, G.R.; Gitto, S.; Sconfienza, L.M. Segmented lordotic angles to assess lumbosacral transitional vertebra on EOS. *Eur. Spine J.* **2020**, *29*, 2470–2476. [[CrossRef](#)] [[PubMed](#)]
14. Deschenes, S.; Charron, G.; Beaudoin, G.; Labelle, H.; Dubois, J.; Miron, M.C.; Parent, S. Diagnostic imaging of spinal deformities: Reducing patients radiation dose with a new slot-scanning X-ray imager. *Spine* **2010**, *35*, 989–994. [[CrossRef](#)] [[PubMed](#)]
15. Bland, J.M.; Altman, D.G. Statistical methods for assessing agreement between two methods of clinical measurement. *Lancet* **1986**, *1*, 307–310. [[CrossRef](#)]
16. Huda, W. Kerma-area product in diagnostic radiology. *AJR. Am. J. Roentgenol.* **2014**, *203*, W565–W569. [[CrossRef](#)] [[PubMed](#)]
17. Di Leo, G.; Sardanelli, F. Statistical significance: P value, 0.05 threshold, and applications to radiomics-reasons for a conservative approach. *Eur. Radiol. Exp.* **2020**, *4*, 18. [[CrossRef](#)] [[PubMed](#)]
18. Albano, D.; Martinelli, N.; Bianchi, A.; Giacalone, A.; Sconfienza, L.M. Evaluation of reproducibility of the MOCART score in patients with osteochondral lesions of the talus repaired using the autologous matrix-induced chondrogenesis technique. *Radiol. Med.* **2017**, *122*, 909–917. [[CrossRef](#)] [[PubMed](#)]

Publisher's Note: MDPI stays neutral with regard to jurisdictional claims in published maps and institutional affiliations.



© 2020 by the authors. Licensee MDPI, Basel, Switzerland. This article is an open access article distributed under the terms and conditions of the Creative Commons Attribution (CC BY) license (<http://creativecommons.org/licenses/by/4.0/>).